International Journal of Mechatronics, Electrical and Computer Technology (IJMEC)
ISSN: 2305-0543 (Online), ISSN: 2411-6173 (Print)
Vol. 12 (45), Jul. 2022, pp. 5233-5237

Improve the resolution of Temporal Averaging Minimum Variance by Sign Coherence Factor: application in photoacoustic imaging

Kian Esmailian
Tehran, Iran
Kian978.esmailian@gmail.com
Tel Number: +98-9127762329

***Abstract*— Photoacoustic (PA) imaging combining the advantages of high resolution of ultrasound imaging and high contrast of optical imaging provides images with good quality. PA imaging often suffers from disadvantages such as clutter noises and decreased signal-to-noise ratio at higher depths. In order to reconstruct an image, Delay-and-Sum (DAS) beamformer is commonly used due to its simplicity and higher robustness compared to other beamformers. However, this beam former's resolution and side lobes rejection are not adequate; in order to address this predicament adaptive beamformer can be used. We used Temporal Averaging Minimum Variance (TAMV) beamformer, which leads to high resolution in this work. Nevertheless, this beamformer could not deter sidelobes. Therefore, Sign Coherence Factor (SCF) was combined with the TAMV beamformer to boost resolution and reject sidelobes.**

Keywords—component; photoacoustic imaging, temporal averaging, sign coherence factor, resolution enhancement

I. INTRODUCTION

A technique that combines the properties of optical and ultrasound imaging (US), photoacoustic imaging (PAI) is an emerging medical imaging technology (Li, 2017) (Junjie & Wang, 2016). PAI is related to the photoacoustic (PA) effect; this combines US and PA properties to provide structural, functional, and potentially the molecular information of tissue (Xia & Wang, 2014) (Mehrmohammadi, Joon Yoon, Yeager, & Emelianov, 2013). An electromagnetic pulse illumination generates acoustic waves due to the thermoelastic effect used for the imaging process (Nasiriavanaki, Xia, Wan, & Bauer, 2013). A reconstruction algorithm is then used to reconstruct the optical absorption distribution map of the tissue (Jeon & Kim, 2013). PAI is a scalable imaging modality used in different preclinical and clinical applications, e.g., ocular imaging (Zerda, Paulus, Teed, & Bodapati, 2010), tumor detection (Guo, Li, Zmuda, & Sheplak, 2007) (Heijblom, Steenbergen, & Manohar, 2015), functional imaging (Nasiriavanaki, Xia, Wan, & Bauer, 2013) (Yao, Xia, Maslov, & Nasiriavanaki, 2013), and monitoring oxygenation in blood vessels (Esenaliev, 2002). Photoacoustic imaging consists of two types: photoacoustic tomography (PAT) and photoacoustic microscopy (PAM) (Zhou, Yao, & Wang, 2016) (Yao & Wang, Photoacoustic microscopy, 2013) (Wang & Hu, 2012). A linear, arc, or circular array of US aperture is used for data recording, and mathematical reconstruction methods are used to create an optical absorption distribution map (Xu & Wang, 2002). There has been a recent surge of interest in PAT and PAM systems that are low-cost (Hariri. 2017).

Delay-and-Sum (DAS) beamformer is commonly used in photoacoustic imaging to reconstruct the desired image. This beamformer does not use intrinsic processing to generate the image. As a result, the image can be reconstructed at a frantic pace; in other words, real-time imagery would be possible by DAS beamformer. It should be noted that this beamformer propels the image into a high level of sidelobes and also poor resolution. Clinicians may get into trouble by the existing sidelobes of the image; thus, their disease diagnosis could be deteriorated (Karaman, Li, & O'Donnell, 1995).

Recently, Delay-Multiply-and-Sum (DMAS) beamformer was proposed in Ultrasound Imaging (UI) (Matrone, Savoia, Caliano, & Magenes, 2015). Before UI, it should be noted that it had been introduced in microwave imaging (Lim et al. 2008). It multiplies the received echoes two-by-two, which mathematically can be interpreted as auto-correlation. The multiplied signals must be added, and finally, a Band-pass Filter (BPF) was applied to the derived signal to keep its second harmonic component and attenuate the DC component (Matrone, Savoia, Caliano, & Magenes, 2015). This beamformer can improve the image quality in terms of sidelobes deterring and resolution, compared to DAS beamformer. Its resolution still is not sufficient. Therefore, some other versions of DMAS beamformer were proposed to ameliorate this setback. Double-stage DMAS (DS-DMAS) beamformer was introduced to reduce sidelobes more than DMAS beamformer (Mozaffarzadeh, Mahloojifar, Orooji, Adabi, & Nasiriavanaki, 2018). This beamformer also can improve the resolution of point targets compared to DMAS. Short-lag DMAS also was a beamformer whose formula was based on a DMAS beamformer (Matrone & Ramalli, 2018). This beamformer considers a lag for multiplication; in other words, it considers fewer coupled signals to generate images. Its resolution enhanced in comparison with the DMAS beamformer; however, the sidelobes enlarged. Lag-DMAS (L-DMAS) beamformer multiplies four signals to reconstruct the image; the sidelobes were rejected more than DMAS beamformer (Song, Liu, & Liu, 2019). It can be concluded that DMAS beamformer and rectified versions could lead to higher resolution and sidelobes rejection; notwithstanding, these are insufficient.

Article History:
Received Date: Mar. 04, 2022, Accepted Date: Jun. 01, 2022, Available Online: Jul. 01, 2022

Coherence Factor (CF) is a beamformer based on the aperture data's spatial spectrum. This beamformer can highly impact the sidelobes and reject them at a high level. Various CF-based beamformers were proposed (Hollman, Rigby, & O'Donnell, 1999). Some examples of which are Modified CF that uses DMAS beamformer in the numerator of CF. It could enhance the sidelobes rejection compared to conventional CF (Mozaffarzadeh, Yan, Mehrmohammadi, & Makkiabadi, 2018). Moreover, Phase CF (PCF) is defined using the standard deviation of the normalized phases of the aperture data (Camacho, Parrilla, & Fritsch, 2009). The Sign (SCF) can be considered a particular case of the PCF and implemented more effectively in the beamformer hardware. SCF can reject sidelobes more than CF (Torbatian, Adamson, Bance, & Brown, 2010). The resolution of CF-based beamformers is restricted, albeit its sidelobes deterring; it could not increase resolution.

In order to address the proposed predicament, adaptive beamformers were proposed. These beamformers make images with high resolution. It also can be said that the resolution considerably enhances by using them compared to DAS beamformer. In particular, minimum variance (MV) can be a suitable option to weight the signals and reduce the effect of the off-axis signals in the reconstructed images (Capon, 1969). This beamformer is highly affected by sidelobes. Eigenspace-based minimum variance (EIG-MV) was proposed to mitigate this drawback, which significantly reduced sidelobes and enhanced resolution (Mohammadzadeh Asl & Mahlooji far, 2010). It has to be noted that CF-based beamformers were combined with adaptive beamformers to increase image quality. An example of this is the combination of CF and MV, which improve sidelobes rejection of MV beamformer (Mohammadzadeh Asl & Mahloojifar, 2009). To supplement this, EIG-MV was combined with SCF to improve sidelobes rejection of EIG-MV and increase SCF resolution (Shamekhi, Periyasamy, Pramanik, Mehrmohammadi, & Mohammadzadeh Asl, 2020).

Temporal Averaging MV (TAMV) is another adaptive beamformer proposed in UI (Mohammadzadeh Asl & Mahloojifar, 2009). This beamformer was not applied to PAI. In this work, we applied TAMV for the first time in PAI; this beamformer could highly boost resolution; nevertheless, this beamformer could be influenced by sidelobes. In order to compensate for this issue, SCF was combined with TAMV. Thus, a new beamformer was proposed, which could enhance both the resolution and sidelobes rejection.

The rest of the paper is organized as follows. Section 2 contains a brief explanation of the TAMV beamformers and the SCF weighting factor and also, the proposed method is introduced in this section. The numerical is illustrated in section 3. Finally, conclusion is given in Section 4.

II. METHOD

A. DAS beamformer

A laser illuminates the imaging target, generating and detecting PA signals. By using a reconstruction algorithm such as DAS, we can reconstruct the PA images. DAS can be written like this:

$$y_{DAS}(k)=\sum_{i=1}^{M} x_i(k-\Delta_i), \quad (1)$$

where y_{DAS} is the output of the DAS beamformer. It was considered that M is the number of elements, and k is the time index. Moreover, Δ_i is the delayed signal for i^{th} transducer.

B. TAMV

The output of a linear array aperture with M elements is as follows:

$$y(k)=W^H(k)x(k)=\sum_{i=1}^{M} w_i(k)x_i(k-\Delta_i), \quad (2)$$

where $w_i(k)$ is related to the adaptive weighting vector related to each element.

Adaptive beamformers such as minimum variance (MV) can be used to reconstruct an image from PA signals. In order to determine MV's optimal weight vector, we need to know:

$$W_{opt}=\frac{R_{i+n}^{-1}a}{a^H R_{i+n}^{-1}a}, \quad (3)$$

where R_{i+n} is the $M^{\times}$M interference-plus-noise covariance matrix and **a** is the steering vector which is vector of ones inasmuch as using the delayed signals.

The exact value of R cannot be provided and hence, the sample covariance matrix is estimated using the spatial averaging over $M - L + 1$ subarrays. Temporal averaging over samples as 2K + 1 also is provided which can be written as:

$$R(k)=\frac{1}{(2k+1)(M-L+1)}\times\sum_{n=-k}^{k}\sum_{l=1}^{M-L+1} x_d^l(k+n)x_d^l(k+n)^H \quad (4)$$

Diagonal loading (DL) was used to obtain stable covariance matrices. White noise is added to the received backscattered echoes by the technique to normalize the optimal weight.

Finally, TAMV can be written as follows:

$$y_{TAMV}(k)=\frac{1}{M-L+1}\sum_{l=1}^{M-L+1} W^H(k)x_d^l(k) \quad (5)$$

C. Proposed algorithm

As aforementioned, in this paper it was desired to achieve a beamformer which could enhance resolution and reject sidelobes. It was claimed that TAMV was not investigated in PAI; thus, in this paper we tried to use this algorithm and enhance its image quality. It was suggested that SCF can be combined with TAMV to improve its performance. SCF can be written as:

$$SCF(k)^p=\left|1-\sqrt{1-[\frac{1}{M}\sum_{i=1}^{M} b_i(k)]^2}\right|^p, \quad (6)$$

IEEE Office - SEET Complex, Federal University of Technology, Owerri, Nigeria, https://aeuso.org
EISSN: 2305-0543, PISSN: 2411-6173

where SCF is the output of desire factor, p can adjust the sensitivity of SCF which must be positive, and b_i is the sign bit that represent the phase of aperture data as shown below:

$$b_i(k) = \begin{cases} -1 & x_i(k) < 0 \\ +1 & x_i(k) \geq 0 \end{cases}. \quad (7)$$

The SCF now can be combined with TAMV beamformer in order to suppress the sidelobes and clutters. The combination of SCF and TAMV can be written as:

$$y_{SCF+TAMV} = SCF \times y_{TAMV} \quad (8)$$

III. Results

In this work, K-wave toolbox (Treeby & Cox, 2010) was used for the simulation setting. A linear transducer was used to record signals which is contained with 64 elements. The sound velocity was assumed to be 1540 m/s, the central frequency was 5MHz, and the bandwidth was set 60%. Five spherical absorbers with 0.1 mm radius are located into axial axis. Imaging region was considered 8mm in lateral axis and 20 mm in axial axis.

For all of simulations, the MV parameters was set to L = 32, k = 10, and diagonal loading factor was 1/100L. Furthermore, white Gaussian noise with SNR of -20 dB was added to signals which inundate image to noise. Finally, the envelope detection and log compression were applied to obtain the final reconstructed images.

A. *In situ point target studies*

Figure (1) demonstrates the performance of DAS, the combination of DAS and SCF, TAMV, and the combination of TAMV and SCF. As seen in this image, DAS beamformer could lead to a high level of sidelobes and poor resolution. The background of the image is also highly influenced by the noise level. As aforesaid, these sidelobes and noises could be destructive for clinicians.

SCF combined DAS beamformer could highly reject sidelobes and also the noise in the background. Thus, this beamformer can attenuate noise level and an image without any sign of noise. As can be seen, this beamformer, especially at higher depths, lead to low resolution.

TAMV beamformer was applied to backscattered signals, and its image was reconstructed. As can be seen, a high level of sidelobes reduces the image quality, and also, a streak of noise can be observed in the background of the image. However, this beamformer significantly improves resolution. It can be said that there is a trade-off between high resolution and sidelobes rejection.

Finally, TAMV was combined with SCF; it is obvious that sidelobes and noises considerably degraded, which improve image quality. Also, this beamformer enhances the resolution of point targets. As a result of that, the proposed method not only increase resolution but also deterring sidelobes.

B. *Lateral Variation*

In order to illustrate the performance of the aforementioned beamformer, lateral variation at 16mm was shown in Figure (2). As can be seen, TAMV leads to high resolution since the main lobe at -6dB is narrower than DAS and SCF beamformers. Also, it is highly affected by sidelobes, but SCF beamformer could reject them outstandingly. DAS beamformer underperformed TAMV and SCF in terms of resolution and sidelobes rejection. At last, the image of TAMV and SCF depicts that this beamformer can attain the highest level of resolution and sidelobes rejection.

Figure. 2 Lateral Variation at 16 mm for DAS, DAS combined SCF, TAMV, and TAMV combined SCF

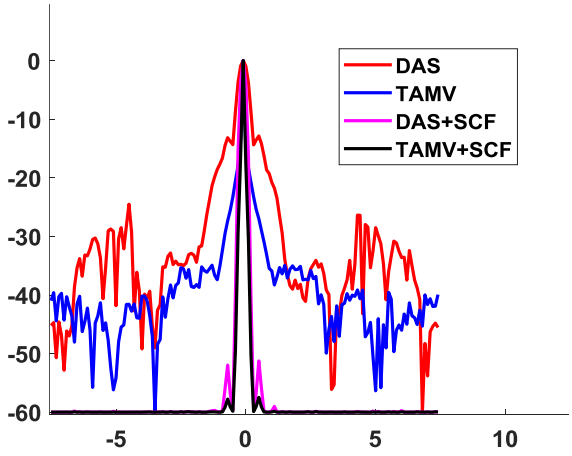

IEEE Office - SEET Complex, Federal University of Technology, Owerri, Nigeria, https://aeuso.org
EISSN: 2305-0543, PISSN: 2411-6173

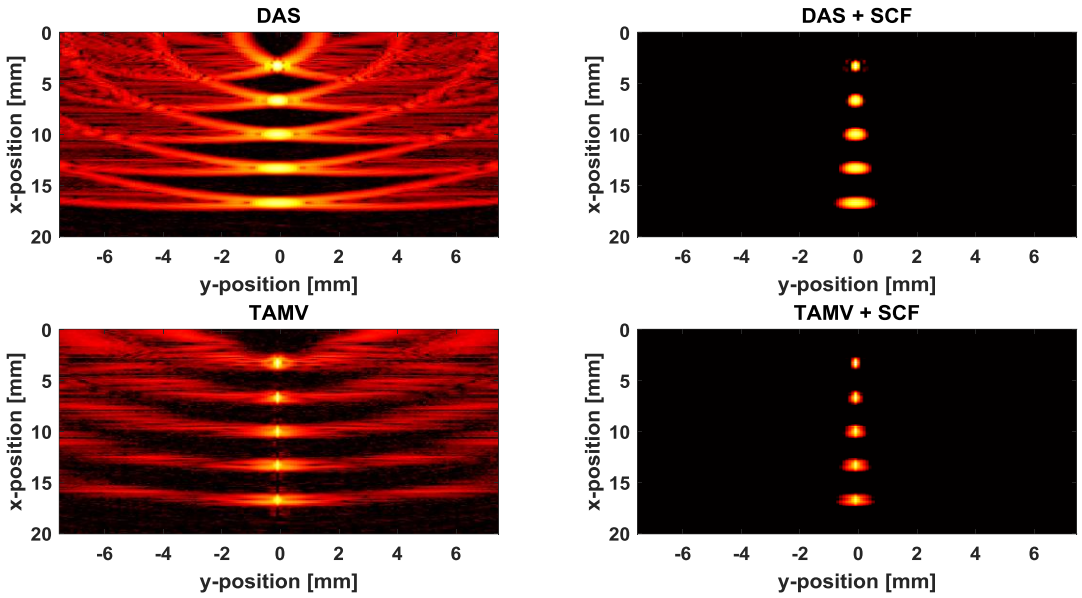

Figure. 1 Simulated 5 point targets using linear array. All the images are displayed of 60dB Dynamic Range.

C. FWHM

The performance of beamformers was evaluated quantitatively. Full-width-half-maximum (FWHM) was calculated for each beamformer at 16mm. Its values can be seen in Table. I. It also can be notified that higher resolution is derived by the combination of TAMV and SCF beamforming algorithm.

TABLE I. FWHM METRIC

	Value			
	DAS	***DAS+SCF***	***TAMV***	***TAMV+SCF***
FWHM	0.5	0.25	0.17	0.13

IV. CONCLUSION

In this study, we applied the SCF to the reconstructed images of the DAS and TAMV beamformers to improve the PA image quality. We have shown that when the SCF is combined with the beamformers, SNR values increase significantly, and at the same time, the mainlobe width is reduced. Between these beamformers, the TAMV presents higher resolution and SNR, and so, the proposed combination of the TAMV and SCF provides images with higher resolution and SNR.

ACKNOWLEDGMENT

The authors are grateful to the anonymous referees for their constructive and insightful comments.

REFERENCES

[1]. Capon, J. (1969). High-resolution frequency-wavenumber spectrum analysis. *IEEE*, 1408-1418.
[2]. R. O. et al (2002). Optoacoustic technique for noninvasive monitoring of blood oxygenation: a feasibility study. *Appl. Opt.* , 4722–4731.
[3]. A.H. et al (2017). Development of low-cost photoacoustic imaging systems using very low-energy pulsed laser diodes. Biomedical Optics.
[4]. Lim. Et al. (2008). Confocal Microwave Imaging for Breast Cancer Detection: Delay-Multiply-and-Sum Image Reconstruction Algorithm. *IEEE Transactions on Biomedical Engineering*, 1697-1704.
[5]. Camacho, J., Parrilla, M., & Fritsch, C. (2009). Phase Coherence Imaging. *IEEE Transactions on Ultrasonics, Ferroelectrics, and Frequency Control*, 958-974.
[6]. Guo, B., Li, J., Zmuda, H., & Sheplak, M. (2007). Multifrequency Microwave-Induced Thermal Acoustic Imaging for Breast Cancer Detection. *IEEE Transactions on Biomedical Engineering*, 2000-2010.
[7]. Heijblom, M., Steenbergen, W., & Manohar, S. (2015). Clinical Photoacoustic Breast Imaging: The Twente experience. *IEEE Pulse*, 42-46.
[8]. Hollman, K. W., Rigby, K. W., & O'Donnell, M. (1999). Coherence factor of speckle from a multi-row probe. *Ultrasonics Symposium. Proceedings. International Symposium* (p. IEEE Ultrasonics Symposium. Proceedings. International Symposium). IEEE.
[9]. Jeon, M., & Kim, C. (2013). Multimodal Photoacoustic Tomography. *IEEE Transactions on Multimedia*, 975-982.
[10]. Junjie , Y., & Wang, L. V. (2016). A practical guide to photoacoustic tomography in the life sciences. *Nature Methods*, 627–638.
[11]. Karaman, M., Li, P.-C., & O'Donnell, M. (1995). Synthetic aperture imaging for small scale systems. *IEEE Transactions on Ultrasonics, Ferroelectrics, and Frequency Control*, 429-442.
[12]. Li, L. (2017). Single-impulse panoramic photoacoustic computed tomography of small-animal whole-body dynamics at high spatiotemporal. *Nat. Biomed. Eng*.

IEEE Office - SEET Complex, Federal University of Technology, Owerri, Nigeria, https://aeuso.org
EISSN: 2305-0543, PISSN: 2411-6173

[13]. Matrone , G., & Ramalli , A. (2018). Spatial Coherence of Backscattered Signals in Multi-Line Transmit Ultrasound Imaging and Its Effect on Short-Lag Filtered-Delay Multiply and Sum Beamforming. *Appl. Sci.*

[14]. Matrone, G., & Ramalli, A. (2018). Spatial Coherence of Backscattered Signals in Multi-Line Transmit Ultrasound Imaging and Its Effect on Short-Lag Filtered-Delay Multiply and Sum Beamforming. *Appl. Sci.*

[15]. Matrone, G., Savoia, A. S., Caliano, G., & Magenes, G. (2015). The Delay Multiply and Sum Beamforming Algorithm in Ultrasound B-Mode Medical Imaging. *IEEE Transactions on Medical Imaging*, 940-949.

[16]. Mehrmohammadi, M., Joon Yoon, S., Yeager, D., & Emelianov, S. (2013). Photoacoustic Imaging for Cancer Detection and Staging. *Current Molecular Imaging*, 89-105.

[17]. Mohammadzadeh Asl, B., & Mahlooji far, A. (2010). Eigenspace-based minimum variance beamforming applied to medical ultrasound imaging. *IEEE Transactions on Ultrasonics, Ferroelectrics, and Frequency Control*, 2381-2390.

[18]. Mohammadzadeh Asl, B., & Mahloojifar, A. (2009). Minimum variance beamforming combined with adaptive coherence weighting applied to medical ultrasound imaging. *IEEE Transactions on Ultrasonics, Ferroelectrics, and Frequency Control*, 1923-1931.

[19]. Mozaffarzadeh, M., Mahloojifar, A., Orooji, M., Adabi, S., & Nasiriavanaki, M. (2018). Double-Stage Delay Multiply and Sum Beamforming Algorithm: Application to Linear-Array Photoacoustic Imaging. *IEEE Transactions on Biomedical Engineering*, 31-42.

[20]. Mozaffarzadeh, M., Yan, Y., Mehrmohammadi, M., & Makkiabadi, B. (2018). Enhanced linear-array photoacoustic beamforming using modified coherence factor. *Biomedical Optics*.

[21]. Nasiriavanaki, M., Xia, J., Wan, H., & Bauer, A. Q. (2013). High-resolution photoacoustic tomography of resting-state functional connectivity in the mouse brain. *PNAS*, 21-26.

[22]. Shamekhi, S., Periyasamy, V., Pramanik, M., Mehrmohammadi, M., & Mohammadzadeh Asl, B. (2020). Eigenspace-based minimum variance beamformer combined with sign coherence factor: Application to linear-array photoacoustic imaging. *Ultrasonics*.

[23]. Song, K., Liu, P., & Liu, D. C. (2019). Lag-Based Filtered-Delay Multiply and Sum Beamformer Combined with Two Phase-Related Factors for Medical Ultrasound Imaging. *Medical & biological engineering & computing*.

[24]. Torbatian, Z., Adamson, R., Bance, M., & Brown, J. A. (2010). A split-aperture transmit beamforming technique with phase coherence grating lobe suppression. *IEEE Transactions on Ultrasonics, Ferroelectrics, and Frequency Control*, 2588-2595.

[25]. Treeby, B. E., & Cox, B. T. (2010). k-Wave: MATLAB toolbox for the simulation and reconstruction of photoacoustic wave fields. *Biomedical Optics*.

[26]. Wang, L. V., & Hu, S. (2012). Photoacoustic Tomography: In Vivo Imaging from Organelles to Organs. *science*, 1458-1462.

[27]. Xia, J., & Wang, L. V. (2014). Small-Animal Whole-Body Photoacoustic Tomography: A Review. *IEEE Transactions on Biomedical Engineering*, 1380-1389.

[28]. Xu, M., & Wang, L. V. (2002). Time-domain reconstruction for thermoacoustic tomography in a spherical geometry. *IEEE Transactions on Medical Imaging*, 814-822.

[29]. Yao, J., & Wang, L. V. (2013). Photoacoustic microscopy. *Laser Photonics Rev.*, 758–778.

[30]. Yao, J., Xia, J., Maslov, K., & Nasiriavanaki, M. (2013). Noninvasive photoacoustic computed tomography of mouse brain metabolism in vivo. *Neuro Image*, 257-266.

[31]. Zerda, A. d., Paulus, Y. M., Teed, R., & Bodapati, S. (2010). Photoacoustic ocular imaging. *Optics Letters*, 270-272.

[32]. Zhou, Y., Yao, J., & Wang, L. V. (2016). Tutorial on photoacoustic tomography. *Biomedical Optics*.

IEEE Office - SEET Complex, Federal University of Technology, Owerri, Nigeria, https://aeuso.org
EISSN: 2305-0543, PISSN: 2411-6173